

Analytical Modeling of Natural Convection in Concentric Spherical Enclosures

P. Teertstra,* M. M. Yovanovich,† and J. R. Culham‡
University of Waterloo, Waterloo, Ontario N2L 3G1, Canada

A modeling procedure is developed for natural convection heat transfer from an isothermal heated sphere located at the center of an isothermal, cooled, spherical-shaped enclosure. The model is based on the linear superposition of conduction and convection solutions, where the convective component is determined based on a combination of two limiting cases, laminar boundary-layer convection and transition flow convection. Validation of the model is performed using experimental and numerical data from the literature. The model and data are shown to be in good agreement, with an rms difference of 2–4%.

Nomenclature

A	= area, m^2
C, \bar{C}_{cs}	= coefficients
d	= diameter, m
$F(Pr)$	= Prandtl number function
G_L	= body gravity function
g	= gravitational acceleration, m/s^2
k	= thermal conductivity, W/mK
k_e	= effective thermal conductivity, $\equiv kNu_L/S_L^*$, W/mK
L	= general characteristic length, m
Nu_L	= Nusselt number, $\equiv QL/(kA_i\Delta T)$
n	= combination parameter
Pr	= Prandtl number, $\equiv \nu/\alpha$
Q	= total heat-transfer rate, W
R	= thermal resistance, $\equiv (T_i - T_o)/Q$, $^\circ\text{C}/\text{W}$
Ra_L	= Rayleigh number, $\equiv g\beta(T_i - T_o)L^3/(\nu\alpha)$
r	= radius, m
S	= conduction shape factor, m
S_L^*	= dimensionless shape factor, $\equiv SL/A_i$
T	= temperature, $^\circ\text{C}$
T_b	= bulk fluid temperature, $^\circ\text{C}$
α	= thermal diffusivity, m^2/s
β	= thermal expansion coefficient, $1/K$
δ	= gap spacing, $\equiv (d_o - d_i)/2$, m
ν	= kinematic viscosity, m^2/s
ϕ	= dimensionless bulk temperature
ψ	= spherical tangential coordinate

Subscripts

b	= bulk fluid
bl	= boundary-layer flow
conv	= convection
i	= inner body

Presented as Paper 2004-496 at the AIAA 42nd Aerospace Sciences Meeting and Exhibit, Reno, NV, 5–8 January 2004; received 24 March 2005; revision received 20 May 2005; accepted for publication 24 May 2005. Copyright © 2005 by the American Institute of Aeronautics and Astronautics, Inc. All rights reserved. Copies of this paper may be made for personal or internal use, on condition that the copier pay the \$10.00 per-copy fee to the Copyright Clearance Center, Inc., 222 Rosewood Drive, Danvers, MA 01923; include the code 0887-8722/06 \$10.00 in correspondence with the CCC.

*Research Assistant Professor, Microelectronics Heat Transfer Lab, Department of Mechanical Engineering; pmt@mhtl.uwaterloo.ca. Member AIAA.

†Distinguished Professor Emeritus, Microelectronics Heat Transfer Lab, Department of Mechanical Engineering; mmyov@mhtl.uwaterloo.ca. Fellow AIAA.

‡Associate Professor, Director MHTL, Microelectronics Heat Transfer Lab, Department of Mechanical Engineering; rix@mhtl.uwaterloo.ca.

LB	= lower bound
o	= outer body
tr	= transition flow
UB	= upper bound

Introduction

NATURAL convection in enclosures has been widely studied both experimentally and analytically by a number of researchers for applications spanning a variety of disciplines, including nuclear reactor design, energy transmission and storage, solar energy, and microelectronics systems. Of particular interest to the designers of electronic equipment for outdoor or harsh environments, including avionics systems, is natural convection in the enclosure formed between a heated body and its surrounding cooled enclosure. The formulation of easy-to-use design tools for the thermal analysis of these equipment provides a mechanism for quickly and accurately predicting operating temperatures and performing tradeoff and parametric studies, prior to more costly and time-consuming computational-fluid-dynamics analysis or prototype testing.

The problem of interest in the current study involves natural convection between an isothermal heated sphere of diameter d_i located at the center of an isothermal, cooled spherical enclosure of diameter d_o , as shown in Fig. 1. This type of enclosure is characterized by a fluid region that has clearly defined, nonintersecting inner and outer boundaries, such that heat transfer occurs between the inner and outer boundaries only. Although not indicative of the more complex geometries found in typical electronics enclosures, the models developed for the concentric spheres will form the basis for future models of more complex enclosure configurations.

Experimental and numerical data for natural convection heat transfer in the concentric spheres have been presented by a number of researchers over the past 40 years. Bishop et al.,^{1,2} Mack and Hardee,³ Scanlan et al.,⁴ and Weber et al.⁵ present experimental data for the concentric spherical enclosure, focusing on the high Rayleigh number, laminar boundary-layer flow regime. Most of the remaining studies involve numerical simulations of the spherical enclosure, including Mack and Hardee,³ Astill et al.,⁶ Caltagirone et al.,⁷ Singh and Chen,⁸ Ingham,⁹ Wright and Douglass,¹⁰ Fujii et al.,¹¹ Garg,¹² Chu and Lee,¹³ and Chiu and Chen.¹⁴ Teertstra et al.¹⁵ present experimental data for four different concentric spheres, $d_o/d_i = 1.5, 2, 3$, and 4.8, measured in a reduced pressure environment, where the resulting change in density leads to a variation in the Rayleigh number of up to five decades from atmospheric conditions. These data will be used to identify trends in the physical behavior of the system, as well as for validation of the completed modeling algorithms.

The parameter of interest in this research study is the total heat-transfer rate Q through the enclosure from the inner to outer boundaries, determined from the temperature gradient in the fluid layer

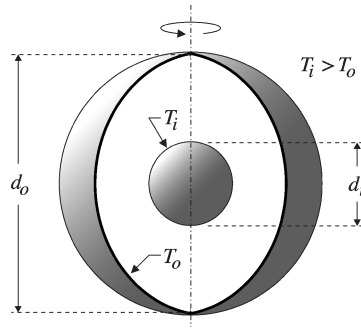


Fig. 1 Schematic of concentric spherical enclosure.

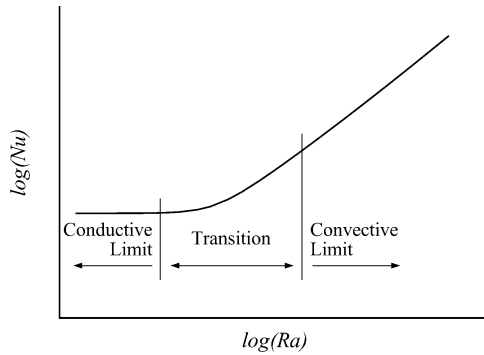


Fig. 2 Schematic of total heat-transfer rate solution trends.

adjacent to the inner body surface:

$$\mathcal{Q} = \iint_{A_i} -k \frac{\partial T}{\partial r} \Big|_{r=r_i} dA_i \quad (1)$$

The total heat-transfer rate is nondimensionalized by the Nusselt number defined using the overall temperature difference ($T_i - T_o$) and an arbitrary scale length \mathcal{L} :

$$Nu_{\mathcal{L}} = \frac{\mathcal{Q}\mathcal{L}}{kA_i(T_i - T_o)} \quad (2)$$

The Rayleigh number is defined using the same overall temperature difference and length scale:

$$Ra_{\mathcal{L}} = \frac{g\beta(T_i - T_o)\mathcal{L}^3}{\nu\alpha} \quad (3)$$

where all fluid properties are evaluated at the bulk temperature T_b .

The numerical data of Astill et al.⁶ for concentric spheres is used to describe the characteristics of the average heat-transfer rate as a function of Rayleigh number. These authors present critical values for the Rayleigh number Ra_{cr} , where the dominant mode of heat transfer changes from conduction to convection. Three distinct regions are identified by Astill et al.,⁶ as shown in Fig. 2: 1) the conduction, or diffusive limit, $Ra \ll Ra_{cr}$, where heat transfer is dominated by conduction, independent of Rayleigh number and equivalent to the dimensionless conduction shape factor, that is, $Nu_{\mathcal{L}} = S_{\mathcal{L}}^*$; 2) the convective limit, $Ra \gg Ra_{cr}$, where heat transfer is dominated by convection at the inner and outer boundaries; and 3) the transition region where values of Nu move smoothly between the limiting cases, typically spanning one to two decades of Ra depending on geometry.

The effective conductivity k_e is an alternate parameter used to quantify the average heat-transfer rate in many studies. It is defined as the apparent value of thermal conductivity required for pure conduction through the enclosed region to be equal to convection. Previous researchers typically present results in terms of dimensionless effective conductivity k_e/k , where k is the actual thermal conductivity of the fluid. The dimensionless effective thermal conductivity is related to the Nusselt number and conduction shape factor $S_{\mathcal{L}}^*$ by

$$k_e/k = Nu_{\mathcal{L}} / S_{\mathcal{L}}^*, \quad k_e/k \geq 1 \quad (4)$$

When dimensionless effective conductivity is used, all results approach a common asymptote $k_e/k \rightarrow 1$ for the conductivity asymptote $Ra < Ra_{cr}$.

Correlations of the experimental and numerical data presented in the literature by Bishop et al.,² Scanlan et al.,⁴ Weber et al.,⁵ Astill et al.,⁶ and Wright and Douglass¹⁰ are valid over a limited range of Rayleigh number, typically corresponding to boundary-layer convection. The only model in the literature for the concentric spheres that is valid for the full range of Rayleigh numbers is presented by Raithby and Hollands¹⁶ in terms of the dimensionless effective conductivity:

$$\frac{k_e}{k} = \bar{C}_{cs} \frac{\delta^{\frac{1}{4}}}{d_i d_o} \frac{Ra_{\delta}^{\frac{1}{4}}}{d_i^{-\frac{7}{5}} + d_o^{-\frac{7}{5}}}, \quad \delta = \frac{d_o - d_i}{2} \quad (5)$$

where the coefficient \bar{C}_{cs} is a combination of the Prandtl number function and an empirically derived coefficient C .

$$\bar{C}_{cs} = C \cdot 0.56 \left(\frac{Pr}{0.846 + Pr} \right)^{\frac{1}{4}} \quad (6)$$

Based on the measurements of Bishop et al.² and Scanlan et al.⁴ for $d_o/d_i = 2$, Raithby and Hollands¹⁶ select a value for the coefficient $C = 1.32$ that provides good agreement between the model and the data. The model is recommended for use when $k_e/k > 1$; for all other cases where values of k_e/k are calculated that are less than one, the conduction limit $k_e/k = 1$ is used.

Comparison of the Raithby and Hollands¹⁶ model for the $d_o/d_i = 2$ concentric spheres with the available numerical data for the transition region reveals that the model underpredicts the data by approximately 10% over the full range to the conduction limit. In the case of larger diameter ratios, such as the $d_o/d_i = 4.8$ experimental data of Teertstra et al.,¹⁵ the underprediction of the Raithby and Hollands¹⁶ model reached 25% near the transition region.

The cause of these differences between the data and the Raithby and Hollands¹⁶ can be traced back to the original two-term analysis of the heat transfer in the enclosure; one term that describes boundary-layer convection at the limit of large Rayleigh number and the other term corresponding to the conduction shape factor solution. Using a piecewise function to combine these expressions results in a model that "switches" from convection to conduction at Ra_{cr} , thereby neglecting the enhancement caused by combined conduction and convection in the transition region.

The goal of the current study is the development of an analytically based modeling procedure for natural convection in the concentric spherical enclosure that is valid over the full range of Rayleigh number, from the conduction limit to the laminar boundary-layer convection limit. The model will be applicable for a wide range of aspect ratios, including the limiting case of the external convection solution $d_o/d_i \rightarrow \infty$ and will not rely on empirically derived correlation coefficients.

Model Development

The previous models of Raithby and Hollands¹⁶ and Kuehn and Goldstein¹⁷ for the two-dimensional circular annulus are based on a combination of two terms: one to quantify heat transfer caused by convection and a second for the conduction limit. These terms can be combined using either the Churchill and Usagi¹⁸ composite technique, such as Kuehn and Goldstein,¹⁷ or in a piecewise fashion, as in Raithby and Hollands.¹⁶ This two-term approach assumes that heat transfer in the enclosure occurs by one of two mechanisms: conduction through the gap or convection through boundary layers on the inner and outer surfaces. When laminar boundary-layer convection is the dominant heat-transfer mode, it is assumed that no interaction occurs between the inner and outer boundary layers. As the Rayleigh number decreases and the boundary layers approach each other, the two-term model assumes a direct transition to conduction-dominated heat transfer occurs.

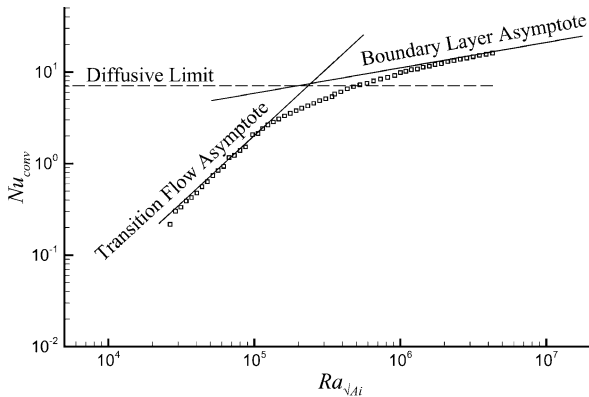


Fig. 3 Convection-only reduced experimental data¹⁵: concentric spheres, $d_o/d_i = 2$.

The experimental data of Teertstra et al.¹⁵ are used to demonstrate that a two-term model is inadequate to describe the heat-transfer process in the enclosure. For natural convection from a heated body in a full-space domain, Yovanovich¹⁹ recommends linear superposition of the convective asymptote with the diffusive limit. Assuming this relationship holds for the enclosure, it is possible to predict the portion of the heat transfer caused by convection from experimental data $Nu_{\sqrt{A_i}}$ using the following relationship:

$$Nu_{\text{conv}} = Nu_{\sqrt{A_i}} - S^*_{\sqrt{A_i}} \quad (7)$$

where the conduction shape factor $S^*_{\sqrt{A_i}}$ is available from the exact solution for conduction in the spherical shell. Convection-only data Nu_{conv} computed by Eq. (7) are presented in Fig. 3 for $d_o/d_i = 2$.

Figure 3 clearly demonstrates that, once the conduction portion of the heat transfer has been reduced from the data, the relationship between Nu_{conv} and $Ra_{\sqrt{A_i}}$ approaches a second asymptotic solution when $Ra_{\sqrt{A_i}} < 3 \times 10^5$. This indicates that an additional term should be incorporated in the existing models to account for changes that occur in the transition region, where boundary layers merge, a velocity distribution is established in the core region, and a transition flow pattern emerges. The general form of this three-term model is

$$Nu_{\sqrt{A_i}} = S^*_{\sqrt{A_i}} + (Nu_{\text{tr}}^{-n} + Nu_{\text{bl}}^{-n})^{-1/n} \quad (8)$$

where the asymptotic solutions for transition flow Nu_{tr} and boundary-layer flow Nu_{bl} are combined using the Churchill and Usagi¹⁸ composite technique. The combination parameter n will be selected based on a comparison with the available experimental data.

The square root of the inner body surface area $\sqrt{A_i}$ has been selected as the characteristic length for the dimensionless quantities based on two criteria. First, for large-aspect-ratio enclosures $d_o/d_i \rightarrow \infty$, heat transfer is controlled by convection at the inner boundary; therefore, the scale length should be related to inner dimensions only and be independent of the outer boundary geometry. Second, Yovanovich¹⁹ and Jafarpur²⁰ have shown that, when $\sqrt{A_i}$ is used, complex geometries can be successfully modeled using equivalent bodies of similar aspect ratio that are more easily characterized. In the following sections component models for each of the asymptotes in Eq. (8) will be developed.

Conduction Shape Factor

The thermal resistance for the concentric spherical shell is determined from a simple conduction analysis in spherical coordinates²¹:

$$R = (1/2\pi k)(1/d_i - 1/d_o) \quad (9)$$

Incorporating the gap thickness δ by substituting $d_o = d_i + 2\delta$ gives

$$R = \delta/\pi k d_i(d_i + 2\delta) \quad (10)$$

The equivalent dimensionless conduction shape factor is determined by

$$S^*_{\sqrt{A_i}} = 1/k\sqrt{A_i}R = \sqrt{\pi}d_i/\delta + 2\sqrt{\pi} \quad (11)$$

Equation (11) represents a linear combination of two limiting cases: for small gap spacing $\delta \ll d_i$, the first term is dominant, corresponding to one-dimensional, planar resistance; as the gap spacing becomes large, $S^*_{\sqrt{A_i}}$ tends to the constant value of a sphere in a full space region $2\sqrt{\pi}$.

Laminar Boundary-Layer Convection

At the limit of large Rayleigh number, assuming the fluid in the core region is of uniform temperature and that the gap spacing δ is large compared to the boundary-layer thickness, the convective heat transfer through the enclosure can be modeled as a series combination of two thermal resistances:

$$R_{\text{conv}} = R_i + R_o \quad (12)$$

where R_i and R_o refer to thermal resistance caused by convection at the inner and outer boundaries, respectively. This total resistance is expressed as a Nusselt number:

$$\begin{aligned} Nu_{\text{bl}} &= (1/k\sqrt{A_i})[1/(R_i + R_o)] \\ &= (1/k\sqrt{A_i})(1/R_i)[1/(1 + R_o/R_i)] \end{aligned} \quad (13)$$

From the definitions of the thermal resistances, the ratio R_o/R_i in Eq. (13) is recast in terms of dimensionless bulk temperature ϕ :

$$\begin{aligned} R_i &= (T_i - T_b)/Q, & R_o &= (T_b - T_o)/Q \\ R_i/R_o &= (T_i - T_b)/(T_b - T_o) = \phi & (14) \end{aligned}$$

Substituting ϕ and $Nu_i = 1/(k\sqrt{A_i}R_i)$ into Eq. (13) gives

$$Nu_{\text{bl}} = Nu_i/(1 + 1/\phi) \quad (15)$$

The convective component at the inner body Nu_i is modeled using the method presented by Yovanovich¹⁹ and Jafarpur²⁰ for natural convection from isothermal, arbitrarily shaped bodies:

$$Nu_{\sqrt{A}} = F(Pr)G_{\sqrt{A}}Ra_{\sqrt{A}}^{\frac{1}{4}} \quad (16)$$

where the Prandtl number function $F(Pr)$ valid for all isothermal body shapes is presented by Churchill and Churchill²²:

$$F(Pr) = \frac{0.67}{[1 + (0.5/Pr)^{9/16}]^{\frac{5}{3}}} \quad (17)$$

and the body gravity function $G_{\sqrt{A}}$ is presented by Lee et al.²³:

$$G_{\sqrt{A}} = \left[\frac{1}{A} \iint_A \left(\frac{P \sin \theta}{\sqrt{A}} \right)^{\frac{1}{3}} dA \right]^{\frac{3}{4}} \quad (18)$$

For the inner body, the convection model is

$$\begin{aligned} Nu_i &= F(Pr)G_{\sqrt{A}}Ra_i^{\frac{1}{4}} \\ Ra_i &= \frac{g\beta(T_i - T_b)(\sqrt{A_i})^3}{\nu\alpha} \\ &= Ra_{\sqrt{A_i}} \left(\frac{T_i - T_b}{T_i - T_o} \right) \\ &= Ra_{\sqrt{A_i}} \frac{1}{[(T_i - T_b)/(T_i - T_b) + (T_b - T_o)/(T_i - T_b)]} \\ &= Ra_{\sqrt{A_i}} \frac{1}{1 + 1/\phi} \end{aligned} \quad (20)$$

Substituting Eqs. (19) and (20) into Eq. (15) and simplifying yields

$$Nu_{bl} = \frac{F(Pr)G\sqrt{A_i}Ra^{\frac{1}{4}}}{(1 + 1/\phi)^{\frac{5}{4}}} \quad (21)$$

Evaluating the dimensionless bulk temperature using the natural convection modeling procedure from Eq. (16) provides the following relationship between ϕ and the enclosure geometry:

$$\begin{aligned} \phi &= \frac{R_i}{R_o} = \frac{\sqrt{A_o}Nu_o}{\sqrt{A_i}Nu_i} \\ &= \frac{\sqrt{A_o}}{\sqrt{A_i}} \frac{G\sqrt{A_o}}{G\sqrt{A_i}} \frac{(T_b - T_o)^{\frac{1}{4}}}{(T_i - T_b)^{\frac{1}{4}}} \frac{(\sqrt{A_o})^{\frac{3}{4}}}{(\sqrt{A_i})^{\frac{3}{4}}} \\ &= \left(\frac{A_o}{A_i} \right)^{\frac{7}{4}} \frac{G\sqrt{A_o}}{G\sqrt{A_i}} \frac{1}{\phi^{\frac{1}{4}}} \end{aligned} \quad (22)$$

Solving Eq. (22) for ϕ and substituting into Eq. (21) results in the general model for the boundary-layer flow convective asymptote:

$$Nu_{bl} = \frac{F(Pr)G\sqrt{A_i}Ra^{\frac{1}{4}}}{\left[1 + (A_i/A_o)^{7/10} \left(G\sqrt{A_i}/G\sqrt{A_o} \right)^{\frac{4}{5}} \right]^{\frac{5}{4}}} \quad (23)$$

For the particular problem of the concentric spherical enclosure, $A_i = \pi d_i^2$, and $A_o = \pi d_o^2$, and the body gravity functions evaluate to

$$G\sqrt{A_o} = G\sqrt{A_i} = 1.014 \quad (24)$$

The general expression for the laminar boundary-layer asymptote can be simplified as follows:

$$Nu_{bl} = \frac{F(Pr)(1.014)Ra^{\frac{1}{4}}}{\left[1 + (d_i/d_o)^{\frac{7}{5}} \right]^{\frac{5}{4}}} \quad (25)$$

All thermofluid properties are evaluated at the bulk fluid temperature, determined by rearranging Eq. (22) in terms of T_b :

$$T_b = \frac{T_i + T_o(d_o/d_i)^{\frac{7}{5}}}{1 + (d_o/d_i)^{\frac{7}{5}}} \quad (26)$$

Transition Flow Convection

The third and final asymptote corresponds to convective heat transfer that occurs in the transition between the conduction and laminar boundary-layer convection limits. As the Rayleigh number decreases, the boundary layers on the inner and outer surfaces of the enclosure grow and eventually merge along the midplane when $Ra < Ra_{cr}$. For Rayleigh number at or below this critical value, the enclosed region can be divided into three regions as shown in Fig. 4: the top-end and bottom-end regions (adjacent to the axis of symmetry) and the central region. The energy equation in spherical coordinates, assuming steady-state, constant properties, axisymmetric geometry, and neglecting frictional heating is

$$u_r \frac{\partial T}{\partial r} + \frac{u_\psi}{r} \frac{\partial T}{\partial \psi} = \alpha \left[\frac{1}{r^2} \frac{\partial}{\partial r} \left(r^2 \frac{\partial T}{\partial r} \right) + \frac{1}{r^2 \sin \psi} \frac{\partial}{\partial \psi} \left(\sin \psi \frac{\partial T}{\partial \psi} \right) \right] \quad (27)$$

When the Rayleigh number is at or below the transition value, heat transfer in the central region is dominated by conduction in the radial direction. As a result, the temperature gradient in the tangential direction $\partial T / \partial \psi$ and velocity in the radial direction u_r

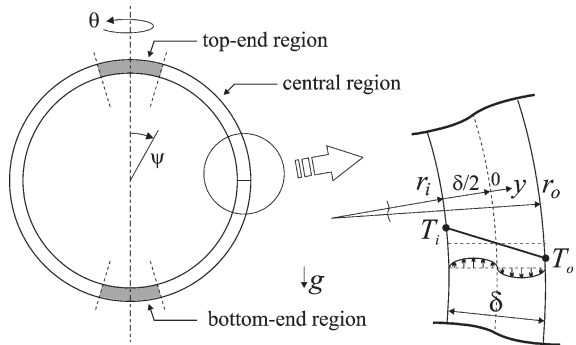


Fig. 4 Transition flow in concentric spherical enclosure.

can be neglected, reducing the energy equation to the familiar one-dimensional Laplace equation in spherical coordinates:

$$\frac{1}{r^2} \frac{d}{dr} \left(r^2 \frac{dT}{dr} \right) = 0 \quad (28)$$

This radial temperature distribution results in a small, buoyancy-induced flow within the region; an upwards flow with respect to the gravity vector in the inner half of the shell and a downwards flow in the outer half. Assuming steady-state, constant properties and an axisymmetric system, the u_ψ momentum equation in spherical coordinates is

$$\begin{aligned} u_r \frac{\partial u_\psi}{\partial r} + \frac{u_\psi}{r} \frac{\partial u_\psi}{\partial \psi} + \frac{u_r u_\psi}{r} &= g \sin \psi \beta (T - T_b) \\ + v \left[\frac{1}{r^2} \frac{\partial}{\partial r} \left(r^2 \frac{\partial u_\psi}{\partial r} \right) + \frac{1}{r^2 \sin \psi} \frac{\partial}{\partial \psi} \left(\sin \psi \frac{\partial u_\psi}{\partial \psi} \right) \right] \end{aligned} \quad (29)$$

As in the case of the energy equation, assuming conduction dominated heat transfer and a fully developed flow pattern in the central region as shown in Fig. 4 results in a simplification of the momentum equation by neglecting the radial velocity $u_r = 0$ and the tangential velocity gradient $\partial u_\psi / \partial \psi = 0$:

$$\frac{1}{r^2} \frac{d}{dr} \left(r^2 \frac{du}{dr} \right) = -\frac{g\beta}{v} \sin \psi (T - T_b) \quad (30)$$

where T_b is the midplane temperature. For the limiting case of narrow gap spacing with respect to the inner and outer boundary dimensions $\delta \ll d_i, d_o$, the governing equations in spherical coordinates can be related to the equivalent problem of flow between vertical plates by defining a local Cartesian coordinate system, as shown in Fig. 4. The radial coordinate is related to the local Cartesian coordinate by

$$r = r_i + \delta/2 + y, \quad i - \delta/2 \leq y \leq \delta/2 \quad (31)$$

and the temperature gradient in spherical coordinates is related to the local coordinate system by

$$\frac{dT}{dr} = \frac{dT}{dy} \frac{dy}{dr} = \frac{dT}{dy} \frac{d}{dr} \left(r - r_i - \frac{\delta}{2} \right) = \frac{dT}{dy} \quad (32)$$

Therefore, at the limit $\delta \ll r_i$ the energy and momentum equations are transformed to the local coordinate system:

$$\frac{1}{r^2} \frac{d}{dr} \left(r^2 \frac{dT}{dr} \right) \rightarrow \frac{d^2 T}{dy^2} = 0 \quad (33)$$

$$\frac{1}{r^2} \frac{d}{dr} \left(r^2 \frac{du}{dr} \right) \rightarrow \frac{d^2 u}{dy^2} = -\frac{g_e \beta}{v} (T - T_b) \quad (34)$$

where $g_e = g \sin \psi$ is the effective gravitation coefficient.

Bird et al.²⁴ and Rohsenow and Choi²⁵ present a solution of these governing equations for the vertical, differentially heated channel.

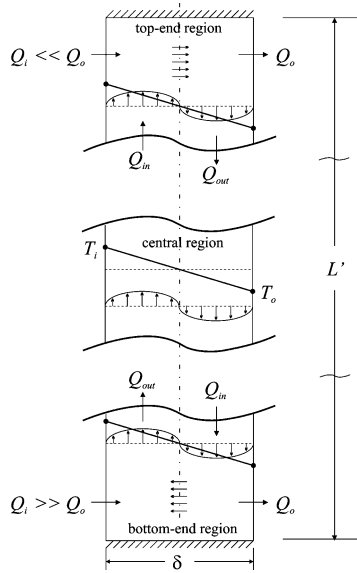


Fig. 5 Schematic of vertical cavity model regions.

Solving the energy equation (33) for isothermal boundary conditions $T(-\delta/2) = T_i$ and $T(\delta/2) = T_o$ gives

$$T - T_b = -[y/(\delta/2)](T_i - T_b), \quad T_b = (T_i + T_o)/2 \quad (35)$$

Substituting this expression into the momentum (34) and solving with a no-slip condition at the wall yields

$$u = (g_e \beta / 12\nu)(T_i - T_o)(\delta/2)^2 \{ [y/(\delta/2)]^3 - y/(\delta/2) \} \quad (36)$$

In the central region, the heat transfer is caused by conduction only, and the linear temperature distribution results in fluid motion caused by buoyancy effects. The addition of the top-end and bottom-end regions to the analysis, as shown in Fig. 5, transforms the vertical parallel plate problem to that of natural convection in a vertical cavity. Batchelor²⁶ and Eckert and Carlson²⁷ present a method for analysis of convective heat transfer in the vertical cavity based on an enthalpy balance within the control volumes formed at the top-end and bottom-end regions, as shown in Fig. 5. For the bottom-end control volume, an enthalpy balance is performed that equates the heat transfer by conduction Q_i and Q_o with the heat transfer through advection by the fluid entering and exiting the control volume from the inner and outer halves of the central region Q_{in} and Q_{out} . The enthalpy flux from the central region Q_{out} is determined based on an integration of the temperature and velocity distributions. For the inner half of the cavity,

$$Q_{out} = \int_{-\delta/2}^0 \rho c_p W' u (T - T_o) dy \quad (37)$$

where W' is the width of the control volume and the temperature rise is defined with respect to the outer wall temperature T_o . Substituting Eqs. (35) and (36) for the temperature and velocity distributions and solving the integral yields

$$Q_{out} = \frac{23}{120} \frac{\rho c_p W' g_e \beta (T_i - T_o)^2 \delta^3}{96\nu} \quad (38)$$

Repeating the analysis for the enthalpy flux for the outer half of the control volume gives

$$Q_{in} = \frac{7}{120} \frac{\rho c_p W' g_e \beta (T_i - T_o)^2 \delta^3}{96\nu} \quad (39)$$

For the bottom-end control volume it is assumed that the boundary layer on the inner, heated surface is much thinner than on the outer, cooled surface, such that $Q_i \gg Q_o$. Therefore, the total enthalpy balance for the bottom-end region is

$$Q_i = Q_{out} - Q_{in} = \frac{\rho c_p W' g_e \beta (T_i - T_o)^2 \delta^3}{720\nu} \quad (40)$$

The analysis for the top-end region control volume yields an equivalent result, with the total heat transfer to the cooled outer surface given by

$$Q_o = Q_{in} - Q_{out} = \frac{\rho c_p W' g_e \beta (T_i - T_o)^2 \delta^3}{720\nu} \quad (41)$$

Therefore, the total heat-transfer rate caused by convection for the transition flow asymptote is equivalent to Q_i in the bottom-end region and Q_o in the top-end region.

The total heat-transfer rate is nondimensionalized by the Nusselt number:

$$Nu_{tr} = \frac{Q \sqrt{A_i}}{k L' W' (T_i - T_o)} \quad (42)$$

where $L' \times W'$ is the cross-sectional area of the equivalent cavity. Substituting Q from the enthalpy balance, Eq. (40), and simplifying the resulting expression yields

$$\begin{aligned} Nu_{tr} &= \frac{1}{720} \frac{\sqrt{A_i}}{L'} \frac{g_e \beta (T_i - T_o) \delta^3}{\nu \alpha} \\ &= \frac{1}{720} \frac{\sqrt{A_i}}{L'} \frac{g_e}{g} \left(\frac{\delta}{\sqrt{A_i}} \right)^3 Ra \sqrt{A_i} \end{aligned} \quad (43)$$

The effective gravitation coefficient is calculated based on an area-weighted integration over a spherical surface at the midplane of the enclosed space:

$$g_e = \frac{1}{A} \iint_A (g \sin \psi) r^2 \sin \psi dA = g \frac{\pi}{4} \quad (44)$$

The ratio of the gap spacing to the inner surface area is easily calculated for the concentric spheres:

$$\delta / \sqrt{A_i} = (d_o - d_i) / 2\sqrt{\pi} d_i \quad (45)$$

The length of the equivalent cavity is determined from an arithmetic average of the inner and outer dimensions $L' = (L_o + L_i)/2$, where effective lengths L_o and L_i that reflect the dimensions and shape of the boundaries are required. Defining the width W according to the maximum perimeter of the body on a plane perpendicular to g provides an upper bound for the Nusselt number:

$$W_{UB} = \pi d, \quad L_{UB} = A/W_{UB} = d \quad (46)$$

The lower bound results from defining the effective length as the distance from the bottom to top stagnation points, or half the perimeter of the body on a plane parallel to the gravity vector:

$$L_{LB} = \pi d/2 \quad (47)$$

The bounds on effective length are combined using a geometric mean:

$$\begin{aligned} L' &= \sqrt{(L_o + L_i)_{UB}(L_o + L_i)_{LB}} \\ &= \sqrt{\frac{1}{2} \cdot (\pi/4)(d_o + d_i)} \end{aligned} \quad (48)$$

Substituting the relationships for effective gravitation coefficient and effective length into Eq. (43) completes the model for the transition flow asymptote:

$$Nu_{tr} = \frac{\sqrt{2/\pi}}{11520} \frac{(d_o/d_i - 1)^3}{(d_o/d_i + 1)} Ra \sqrt{A_i} \quad (49)$$

Model Validation

The natural convection model developed in the preceding section is validated using the experimental data of Teertstra et al.¹⁵ and other numerical and experimental data from the literature for a wide range of diameter ratios and Rayleigh number. A combination parameter value $n = 2$ was selected, which provides a good fit to the experimental data of Teertstra et al.¹⁵

Figure 6 compares the convection-only portion of the model with the experimental data of Teertstra et al.¹⁵ reduced using Eq. (7), where $S_{\sqrt{A_i}}^*$ is the exact solution for conduction shape factor in the concentric spherical shell. This comparison with the composite model for the convection terms is used in the selection of a combination parameter $n = 2$, which provides good agreement of the model with the data throughout the transition region. The larger differences shown in Fig. 6 as the Rayleigh number decreases further are caused by uncertainty in the experimental data, which becomes more significant as $Nu_{\sqrt{A_i}} \rightarrow S_{\sqrt{A_i}}^*$ and $Nu_{\text{conv}} \rightarrow 0$.

The full model is compared with the experimental data of Teertstra et al.¹⁵ for four different concentric spherical enclosures, $d_o/d_i = 1.5, 2, 3$, and 4.8 , in Fig. 7. This plot shows the excellent agreement between the model and the data, with the model successfully following the trends of the data and the transition from conduction to convection-dominated heat transfer occurring at different Rayleigh numbers depending on the diameter ratio. The overall rms difference between the data and the model is 3–4%, with a maximum difference of 7%. A full list of the percent differences is given in Table 1.

Figures 8–10 compare the model with existing numerical and experimental data from the literature for a wide range of diameter ratio from the $d_o/d_i = 1.03$ numerical data of Astill et al.⁶ presented in Fig. 8 to the $d_o/d_i = 50$ numerical data of Fujii et al.¹¹ in Fig. 10. The model and data are in good agreement in all cases presented in

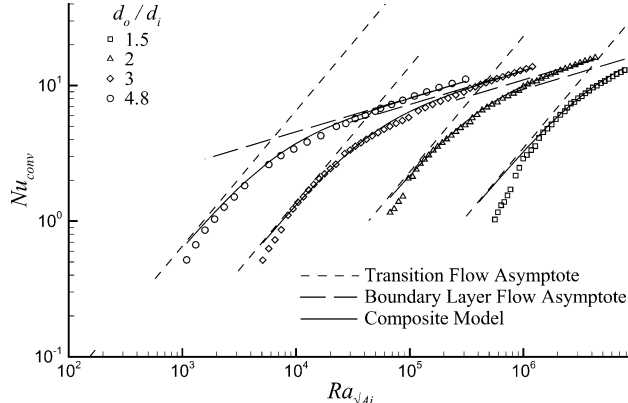


Fig. 6 Convection-only model validation with experimental data of Teertstra et al.¹⁵

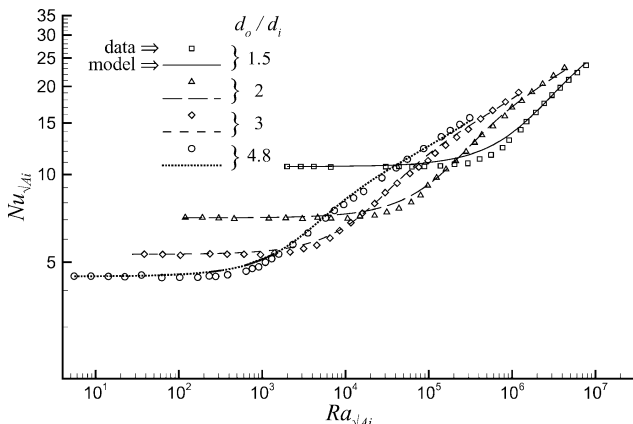


Fig. 7 Model validation with Teertstra et al.¹⁵

Table 1 Comparison of model predictions vs data¹⁵

d_o/d_i	rms, %	Max, %
1.5	4.3	7.3
2	3.0	5.8
3	2.3	4.9
4.8	2.8	4.9

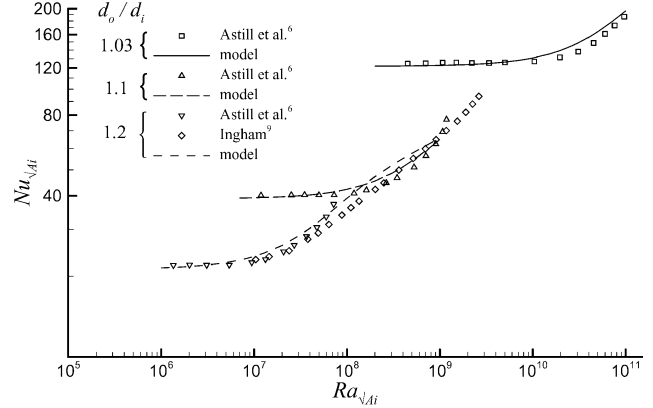


Fig. 8 Model validation with previous data: $d_o/d_i \leq 1.2$.

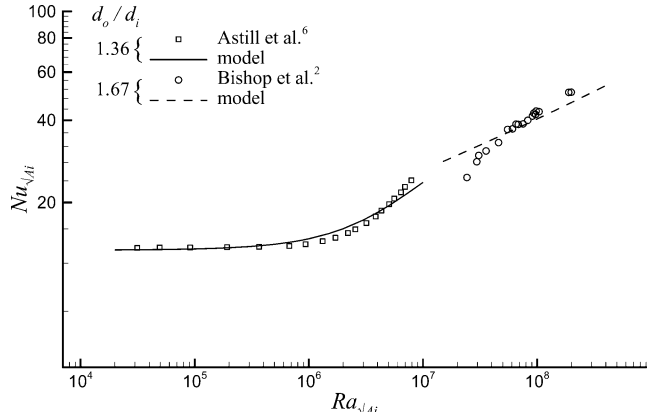


Fig. 9 Model validation with previous data: $1.25 \leq d_o/d_i < 2$.

Figs. 8–10. The large amount of scatter in the experimental data of Bishop et al.² makes it difficult to provide an accurate fit of all of the data points; however, both Figs. 9 and 10 demonstrate that the model is in good agreement with the majority of the data. Figure 8 also compares the model with the experimental measurements of Chamberlain²⁸ for an isothermal sphere in a full space domain, a limiting case of the concentric spherical enclosure $d_o/d_i \rightarrow \infty$, for which the three-term model is in excellent agreement.

The majority of the numerical and experimental data presented in the literature involves the $d_o/d_i = 2$ concentric spherical enclosure, and all available data for this configuration are compared with the model predictions in Fig. 11. All of these data represent the result of numerical simulations with the exception of the experimental data of Bishop et al.² All of these data are in good agreement with each other, with the majority of the data within $\pm 5\%$ for $Ra_{\sqrt{A_i}} < 10^6$. As can be seen from Fig. 11, the three-term natural convection model provides excellent agreement with the data over the full range of Rayleigh numbers, from the numerical conduction limit data of Garg¹² through the transition region to the experimental laminar boundary-layer data of Bishop et al.²

Also included in Fig. 11 is the two-term model of Raithby and Hollands,¹⁶ which provides an effective fit of the data for high values of Rayleigh numbers $Ra_{\sqrt{A_i}} \approx 10^7$; however, for $Ra_{\sqrt{A_i}} \leq 10^6$ this model underpredicts the data by approximately 10% over the full range to the conduction limit. The piecewise method used by

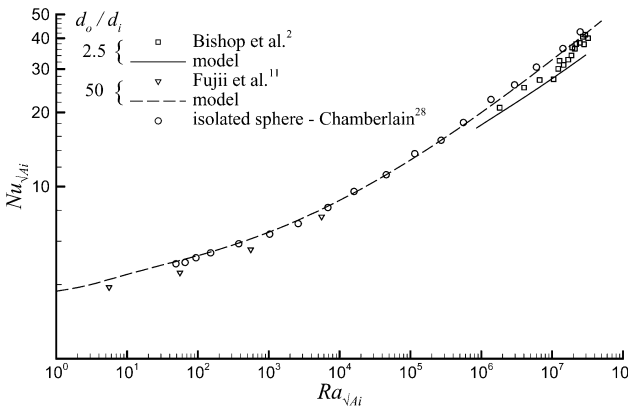


Fig. 10 Model validation with previous data: $d_o/d_i \geq 2.5$.

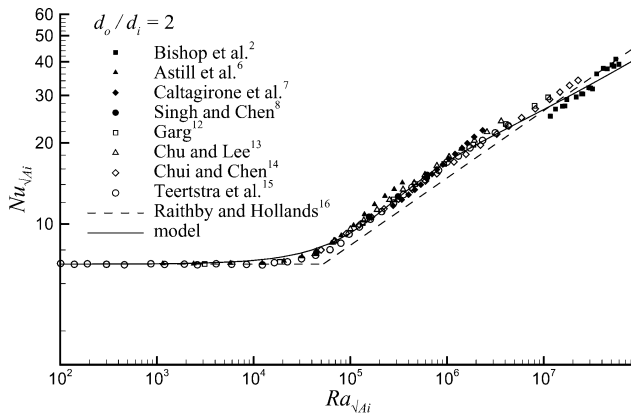


Fig. 11 Model validation with previous data and models: $d_o/d_i = 2$.

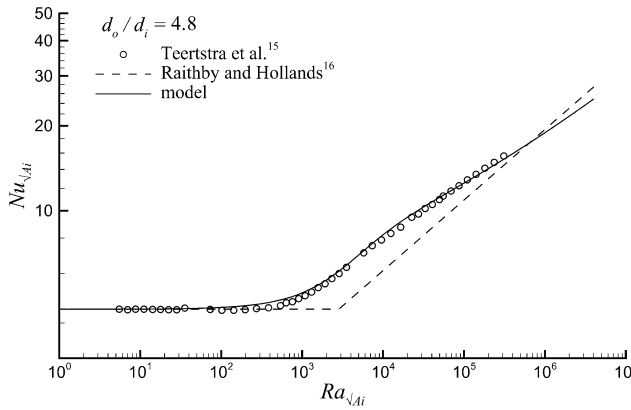


Fig. 12 Model validation with previous data and models: $d_o/d_i = 4.8$.

Raithby and Hollands¹⁶ results in a model that neglects the contribution of conduction to the heat transfer for intermediate values of Rayleigh number in the transition region.

The model and data of Teertstra et al.¹⁵ for $d_o/d_i = 4.8$ are compared with the model of Raithby and Hollands¹⁶ in Fig. 12. As in the preceding plot, Fig. 12 demonstrates that the two-term model of Raithby and Hollands¹⁶ underpredicts both the model and the data, with a maximum difference of 25% at Ra_{cr} .

Summary

A model has been developed for natural convection heat transfer in the concentric spherical enclosure with isothermal conditions on the inner (heated) and outer (cooled) boundaries. The model is based on three limiting case solutions, corresponding to the diffusive limit, laminar boundary-layer convection, and transition flow convection. A full validation with published numerical and experimental results

has demonstrated the effectiveness of the model for a wide range of diameter ratios and Rayleigh number, with an average rms difference of 2–3%. Because it is formed based on asymptotic solutions for limiting geometry cases, the model is applicable to a wide range of diameter ratios; however, because the model has been validated using air data only it is recommended that only fluids with Prandtl number values near unity be considered. The modeling procedure developed for this fundamental geometry will provide the basis for future analyses of more complex enclosure configurations.

Acknowledgments

The authors acknowledge the continued financial support of Materials and Manufacturing Ontario (MMO) and the Centre for Microelectronics Assembly and Packaging (CMAP).

References

- ¹Bishop, E. H., Kolflat, R. S., Mack, L. R., and Scanlan, J. A., "Convective Heat Transfer Between Concentric Spheres," *Proceedings of the 1964 Heat Transfer and Fluid Mechanics Institute*, edited by W. H. Giedt and S. Levy, Stanford Univ. Press, Stanford, CA, 1964, pp. 69–80.
- ²Bishop, E. H., Mack, L. R., and Scanlan, J. A., "Heat Transfer by Natural Convection Between Concentric Spheres," *International Journal of Heat and Mass Transfer*, Vol. 9, No. 7, 1966, pp. 649–662.
- ³Mack, L. R., and Hardee, H. C., "Natural Convection Between Concentric Spheres at Low Rayleigh Numbers," *International Journal of Heat and Mass Transfer*, Vol. 11, No. 3, 1968, pp. 387–396.
- ⁴Scanlan, J. A., Bishop, E. H., and Powe, R. E., "Natural Convection Heat Transfer Between Concentric Spheres," *International Journal of Heat and Mass Transfer*, Vol. 13, No. 12, 1970, pp. 1857–1872.
- ⁵Weber, N., Powe, R. E., Bishop, E. H., and Scanlan, J. A., "Heat Transfer by Natural Convection Between Vertically Eccentric Spheres," *Journal of Heat Transfer*, Vol. 95, No. 1, 1973, pp. 47–52.
- ⁶Astill, K. N., Leong, H., and Martorana, R., "A Numerical Solution for Natural Convection in Concentric Spherical Annuli," *Natural Convection in Enclosures*, American Society of Mechanical Engineers, New York, Vol. 8, 1980, pp. 105–113.
- ⁷Caltagirone, J.-P., Combarous, M., and Mojtabi, A., "Natural Convection Between Two Concentric Spheres: Transition Toward a Multicellular Flow," *Numerical Heat Transfer*, Vol. 3, No. 1, 1980, pp. 107–114.
- ⁸Singh, S. H., and Chen, J., "Numerical Solution for Free Convection Between Concentric Spheres at Moderate Grashof Numbers," *Numerical Heat Transfer*, Vol. 3, No. 4, 1980, pp. 441–459.
- ⁹Ingham, D. B., "Heat Transfer by Natural Convection Between Spheres and Cylinders," *Numerical Heat Transfer*, Vol. 4, No. 1, 1981, pp. 53–67.
- ¹⁰Wright, J. L., and Douglass, R. W., "Natural Convection in Narrow-Gap, Spherical Annuli," *International Journal of Heat and Mass Transfer*, Vol. 29, No. 5, 1986, pp. 725–739.
- ¹¹Fujii, M., Takamatsu, H., and Fujii, T., "A Numerical Analysis of Free Convection Around an Isothermal Sphere (Effects of Space and Prandtl Number)," *Proceedings of the 1987 ASME/JSME Thermal Engineering Joint Conference*, edited by J. Marto and I. Tanasawa, Vol. 4, 1987, pp. 55–60.
- ¹²Garg, V. K., "Natural Convection Between Concentric Spheres," *International Journal of Heat and Mass Transfer*, Vol. 35, No. 8, 1992, pp. 1935–1945.
- ¹³Chu, H.-S., and Lee, T.-S., "Transient Natural Convection Heat Transfer Between Concentric Spheres," *International Journal of Heat and Mass Transfer*, Vol. 36, No. 13, 1993, pp. 3159–3170.
- ¹⁴Chiu, C. P., and Chen, W. R., "Transient Natural Convection Heat Transfer Between Concentric and Vertically Eccentric Spheres," *International Journal of Heat and Mass Transfer*, Vol. 39, No. 7, 1996, pp. 1439–1452.
- ¹⁵Teertstra, P., Yovanovich, M. M., and Culham, J. R., "Natural Convection Measurements for a Concentric Spherical Enclosure," Paper No. 32974, IMECE Conference, American Society of Mechanical Engineers, New York, Nov. 2002.
- ¹⁶Raithby, G. D., and Hollands, K. G. T., "A General Method of Obtaining Approximate Solutions to Laminar and Turbulent Free Convection Problems," *Advances in Heat Transfer*, edited by T. F. Irvine, Jr., and J. P. Hartnett, Vol. 11, Academic Press, New York, 1975, pp. 265–315.
- ¹⁷Kuehn, T. H., and Goldstein, R. J., "Correlating Equations for Natural Convection Heat Transfer Between Horizontal Circular Cylinders," *International Journal of Heat and Mass Transfer*, Vol. 19, No. 10, 1976, pp. 1127–1134.
- ¹⁸Churchill, S. W., and Usagi, R., "A General Expression for the Correlation of Rates of Transfer and Other Phenomenon," *American Institute of Chemical Engineers Journal*, Vol. 18, No. 6, 1972, pp. 1121–1128.
- ¹⁹Yovanovich, M. M., "New Nusselt and Sherwood Numbers for Arbitrary Isopotential Geometries at Near Zero Peclet and Rayleigh Numbers," *AIAA Paper 87-1643*, 1987.

²⁰Jafarpur, K., "Analytical and Experimental Study of Laminar Free Convective Heat Transfer from Isothermal Convex Bodies of Arbitrary Shape," Ph.D. Dissertation, Dept. of Mechanical Engineering, Univ. of Waterloo, Ontario, Canada, 1992.

²¹Incropera, F. P., and DeWitt, D. P., *Fundamentals of Heat and Mass Transfer*, 4th ed., Wiley, New York, 1996, pp. 96–99, 114–118.

²²Churchill, S. W., and Churchill, R. U., "A Comprehensive Correlating Equation for Heat and Component Heat Transfer by Free Convection," *American Institute of Chemical Engineers Journal*, Vol. 21, No. 3, 1975, pp. 604–606.

²³Lee, S., Yovanovich, M. M., and Jafarpur, K., "Effects of Geometry and Orientation on Laminar Natural Convection Heat Transfer from Isothermal Bodies," *Journal of Thermophysics and Heat Transfer*, Vol. 5, No. 2, 1991, pp. 208–216.

²⁴Bird, R. B., Stewart, W. E., and Lightfoot, E. N., *Transport Phenomena*, Wiley, New York, 1960, pp. 297–300.

²⁵Rohsenow, W. M., and Choi, H. Y., *Heat, Mass and Momentum Transfer*, Prentice-Hall, Upper Saddle River, NJ, 1961, pp. 143–146.

²⁶Batchelor, G. K., "Heat Transfer by Free Convection Across a Closed Cavity Between Vertical Boundaries at Different Temperatures," *Quarterly of Applied Mathematics*, Vol. 12, No. 3, 1954, pp. 209–223.

²⁷Eckert, E. R. G., and Carlson, W. O., "Natural Convection in an Air Layer Enclosed Between Two Vertical Plates with Different Temperatures," *International Journal of Heat and Mass Transfer*, Vol. 2, No. 2, 1961, pp. 106–120.

²⁸Chamberlain, M. J., "Free Convection Heat Transfer from a Sphere, Cube and Vertically Aligned Bi-Sphere," M.A.Sc. Thesis, Dept. of Mechanical Engineering, Univ. of Waterloo, Ontario, Canada, 1983.